Journal of Thermal Science

**https://doi.org/10.1007/s11630-022-1632-7**

# Performance Assessment of Low-Temperature A-CAES (Adiabatic Compressed Air Energy Storage) Plants

**TOLA Vittorio*, MARCELLO Francesca Carolina, COCCO Daniele, CAU Giorgio**

Department of Mechanical, Chemical and Materials Engineering, University of Cagliari, 09123 Cagliari, Italy



**Abstract:** The widespread diffusion of renewable energy sources calls for the development of high-capacity energy storage systems as the A-CAES (Adiabatic Compressed Air Energy Storage) systems. In this framework, low temperature (100°C–200°C) A-CAES (LT-ACAES) systems can assume a key role, avoiding some critical issues connected to the operation of high temperature ones.

In this paper, two different LT-ACAES configurations are proposed. The two configurations are characterized by the same turbomachines and compressed air storage section, while differ in the TES section and its integration with the turbomachinery. In particular, the first configuration includes two separated cycles: the working fluid (air) cycle and the heat transfer fluid (HTF) cycle. Several heat exchangers connect the two cycles allowing to recover thermal energy from the compressors and to heat the compressed air at the turbine inlet. Two different HTFs were considered: air (case A) and thermal oil (case B). The second configuration is composed of only one cycle, where the operating fluid and the HTF are the same (air) and the TES section is composed of three different packed-bed thermal storage tanks (case C). The tanks directly recover the heat from the compressors and heat the air at each turbine inlet, avoiding the use of heat exchangers.

The LT-ACAES systems were modelled and simulated using the ASPEN-Plus and the MATLAB-Simulink environments. The main aim of this study was the detailed analysis of the reciprocal influence between the turbomachinery and the TES system; furthermore, the performance evaluation of each plant was carried out assuming both on-design and off-design operating conditions. Finally, the different configurations were compared through the main performance parameters, such as the round-trip efficiency.

A total power output of around 10 MW was set, leading to a TES tank volume ranging between 500 and 700 $m^3$. The second configuration with three TES systems appears to be the most promising in terms of round-trip efficiency since the energy produced during the discharging phase is greater. In particular, the round-trip efficiency of the LT-ACAES ranges between 0.566 (case A) to 0.674 (case C). Although the second configuration assures the highest performance, the effect of operating at very high pressures inside the tanks should be carefully evaluated in terms of overall costs.

**Keywords: compressed air energy storage, low temperature A-CAES, Thermal Energy Storage, system integration**

Article Type: Contributed by the International Conference on Efficiency, Cost, Optimization, Simulation & Environmental Impact of Energy Systems (ECOS 2021) GE: SUN Jie
Received: Oct 30, 2021 Corresponding author: TOLA Vittorio E-mail: vittorio.tola@unica.it

| **Nomenclature** | | | |
|---|---|---|---|
| A-CAES | Adiabatic compressed air energy storage | PHES | Pumped hydroelectric storage |
| CAES | Compressed air energy storage | TES | Thermal Energy Storage |
| CAS | Compressed air storage | THP | High-pressure turbine |
| CHP | High-pressure compressor | TIP | Intermediate pressure turbine |
| CIP | Intermediate-pressure compressor | TIT | Turbine inlet temperature |
| CLP | Low-pressure compressor | TLP | Low-pressure turbine |
| CVHP | Very high-pressure compressor | TOT | Turbine outlet temperature |
| D-CAES | Diabatic compressed air energy storage | **Greek symbol** | |
| HTF | Heat transfer fluid | $\beta$ | Pressure ratio |
| LT-ACAES | Low temperature adiabatic compressed air energy storage | | |

## 1. Introduction

Worldwide, the production of electricity from intermittent and fluctuating renewable energy sources has largely increased in the last decade. In 2019, the share of renewables in the global electricity supply reached 27% [1]. This great increase has called for the development of suitable energy storage systems to support and improve the efficiency of electrical grids [2]. In fact, energy storage systems allow to temporarily decouple the production and the consumption of electricity by converting electrical energy into an easier storable form of energy such as chemical, mechanical, or electrochemical [3]. In particular, energy storage systems bring different benefits to the electrical grids such as load levelling and peak shaving, ensuring that the energy supply matches the energy demand. Moreover, energy storage favors the frequency regulation, the decrease of energy oscillations, and the improvement of power quality and reliability [3]. Nowadays, various energy storage technologies are available. In the field of large capacity systems, pumped hydroelectric storage (PHES) plants take the lead among the mechanical ones, while the compressed air energy storage (CAES) systems are a promising alternative. In fact, CAES plants allow to store a large amount of energy as compressed air with lower specific investment costs [4, 5]. The rating power of CAES plants can range between 1 MW to 1 GW, while the CAES cycle efficiency ranges between 0.42 to 0.7, depending on the configuration [6]. The estimated lifespan of a CAES plant is 30 years long, allowing more than $10^4$ cycles, while the discharge duration ranges between 1 h and 12 h [4]. These characteristics make the CAES systems suitable for various tasks, as, for example, time shifting, peak shaving, load levelling, seasonal storage, and energy management [7]. In the 70s, two large-size commercial plants, still operating (Huntorf [8] in Germany and McIntosh [9] in US), have been implemented. After a long stagnation period, in the last decade the interest and research activities concerning CAES are increasing [10–14].

A CAES system is composed of a series of compressors and turbines, a compressed air storage (CAS) reservoir, an electric motor/generator, and a compressed air heating system. The CAES system works in two phases, namely the charge and the discharge [15]. During the charge, electricity from the grid is used to compress air that is then stored in the compressed air storage reservoir at high pressure (typically ranging between 6.0 and 10.0 MPa [16]). The energy production (discharge) phase consists of the release of the compressed air from the CAS, the air heating, and the expansion in a conventional gas turbine to generate electricity [6]. The CASs are mainly isochoric and can be artificial or natural. For small size plants, artificial ones such as pressure vessels or piping are preferred, while for larger scale plants natural CASs, such as salt caverns (already used by the two existing plants), are more suitable. The availability of suitable CASs also represents a possible obstacle for the spread of CAES systems, due to possible structural issues inside the artificial CASs and for natural ones, due to geological restrictions and the necessity to build the system in a particular region depending on the CAS availability [6, 17].

The CAES arrangements mainly differ in the compressed air heating principle. The conventional diabatic CAES (D-CAES) systems, like the two existing commercial plants, require a combustion chamber to heat the compressed air during the discharge. In more advanced configurations, the system is integrated with a regenerative heat exchanger to partially recover the thermal energy of the turbine exhaust. Coupling the CAES system with renewable energy sources calls for the shifting to the more advanced adiabatic CAES (A-CAES) concept. In such systems, during the charging phase the thermal energy of the compressed air available at the compressors exit is recovered and the introduction of a thermal energy storage (TES) system allows to

eliminate the use of fuels and to avoid the related $CO_2$ emissions [18]. In fact, the stored thermal energy is used during the generation phase to heat the compressed air coming from the reservoir, avoiding the consumption of fuel. The TES system can be based on different storage media, such as thermal oil [19], phase change materials [20] or solid materials [21]. Although the heat recovery leads to performance improvements, the process involves some technological, thermodynamic, and operational issues, including the off-design behavior of system components and the most suitable choice of both storage technology and materials.

Depending on the storage temperature of the TES, different conceptual arrangements of A-CAES are considered: the low temperature (100°C–200°C), the medium-temperature (200°C–500°C) and the high temperature (500°C–600°C) A-CAES. In the last decade, the European research project ADELE has been developed with the aim of realizing an advanced A-CAES with high-temperature storage. However, the realization of a high-temperature A-CAES encounters two main issues: the thermal and mechanical stress in the TES tank, due to the high temperature and the necessity to develop specific compressors able to reach such high temperature, since, currently, this is not an off-the-shelf available technology. In comparison to PHES plants, these systems require a larger start-up time (about 10 minutes, instead of the 2 min of PHESs), but on the other hand, they provide major flexibility, since the turbines are based on conventional gas turbines. In medium-temperature A-CAES the energy from the charging phase is usually stored inside two different TES tanks, with molten salt or oil as heat transfer fluids. Medium-temperature configuration allows to use already existing technology for the compressors, while the start-up time is still of about 10 minutes. As a matter of fact, medium- and high-temperature A-CAES systems lead to better performance than low-temperature options. However, low-temperature A-CAES (LT-ACAES) systems allow avoiding some critical issues connected to the operation of the higher temperature ones, such as the thermal stress in the TES tanks and the necessity to design new and specific compressors to reach very high temperatures. Moreover, the low-temperature CAES systems require a start-up time of only 5 minutes that makes this technology suitable as secondary control reserve. Therefore, low-temperature A-CAES systems result in a good compromise between a simpler design, due to the use of existing technologies, and lower performance, due to both the lower temperature of the cycle and the presence of numerous heat exchangers [6].

In this study, two different LT-ACAES configurations have been analyzed, the main difference being the choice of the system used: (1) to recover the thermal energy from the air compression process, (2) to store it and (3) to utilize it by heating the compressed air before the expansion. In particular, in the first configuration the heat recovery is carried out through several heat exchangers using air or oil (Therminol 66) as heat transfer fluid (HTF) [22], while in the second one the A-CAES working fluid (air) directly feeds a TES system. The proposed LT-ACAES plant was sized to achieve a maximum power output equal to 10 MW in the best performing configuration studied. To the best knowledge of the authors, there is a shortage of studies concerning the analysis of the off-design behavior of an overall LT-ACAES plant. In literature, other studies analyzed a LT-ACAES plant integrated with a solid packed bed, as, for example, Barbour and al. [21], but just limiting the off-design analysis to the TES system. The main novelty of this work involves an in-depth study of the off-design behavior of both the mechanical and thermal energy storage sections composing the LT-ACAES and their mutual interactions. As in a previous paper of the same authors [16], regarding high-temperature A-CAES plants, this work proposes a novel A-CAES configuration characterized by: (i) three centrifugal compressors constantly operating at design conditions and a further centrifugal compressor for the complete management of the CAS back-pressure variation, (ii) a direct or indirect TES system based on packed beds of solid particles (and on heat exchangers in the case of indirect configuration), located downstream of each axial compressor, (iii) an expansion train based on three radial turbines.

The A-CAES systems were studied through dedicated simulation models. In particular, the commercial code Aspen-Plus was used for the CAES plant, whereas a specific MATLAB-Simulink code was used to simulate the TES systems. The evaluation of the plant performance was carried out assuming both on-design and off-design operating conditions. The main aim of this study was to explore the mutual influence between the turbomachinery and the TES system operation. Furthermore, the different configurations proposed were compared through the evaluation of the main performance parameters, such as the round-trip efficiency.

## 2. Plant Configuration

The A-CAES system operates alternatively in charging and discharging mode. During the charging phase, the air is compressed up to the maximum operating pressure by four compressors. The air exiting each of the first three compressors (the low-pressure CLP, the intermediate-pressure CIP and the high-pressure CHP ones) is cooled in a heat exchanger or directly in a TES system, depending on the configuration. Then, the recovered thermal energy is stored in a packed-bed TES system, at a temperature ranging between 150°C and 170°C, to be used during the discharging phase. The very

high-pressure compressor CVHP allows to overcome the existing backpressure in the CAS system (a cave, for example), by varying its discharging pressure from 6.4 to 10.0 MPa, set as minimum and maximum pressure, according to typical CAES pressure ranges [16]. Then the compressed air is stored in the CAS system to be subsequently extracted during the discharging phase. To avoid structural issues in the cave, an aftercooler is introduced downstream of the CVHP to cool the air.

During the discharging phase, the compressed air expands through three turbines (the high-pressure THP, the intermediate-pressure TIP and the low-pressure TLP) from the cave pressure to the ambient pressure. Before entering each turbine, the air is heated exploiting the thermal energy stored in the TES system. A valve, at the entrance of each turbine, allows reducing the air pressure if necessary, avoiding an exhaust temperature lower than 15°C, set as the minimum reference value. Since the compression and expansion processes take place separately, turbines and compressors can be coupled on different shafts.

Since the system was supposed to store electrical energy from photovoltaic plants, a charging phase of 6 hours was assumed, whereas a duration of the discharging phase equal to 3 hours was established to cover daily peak loads. Starting from the assumptions on the main turbine parameters reported later, a turbine air mass flow rate slightly lower than 25 kg/s is required to achieve the maximum power output of 10 MW. Considering the above-mentioned ratio of charge/discharge duration, the cave mass balance leads to an air mass flow rate of the compression train equal to half of the one requested by the expansion train.

The two analysed configurations are similar in terms of turbomachinery and CAS, while the main differences are related to the TES section and to its integration with the turbomachinery. The first configuration is based on two separated cycles: the working fluid (air) cycle and the HTF cycle. The system includes several heat exchangers to recover thermal energy from the compressors exit during the charging phase and to heat the compressed air at the turbine inlet during the discharging phase [23–26]. Two different HTFs were considered: air (case A) and thermal oil (Therminol 66) (case B). Since the two cycles are separated, in this configuration the TES system can operate at atmospheric pressure. In the second configuration (case C), the working fluid and the HTF are the same (air) and the TES system is composed of three packed-bed tanks operating at different pressures. Each tank is directly fed by the hot air from a compressor during the charging phase and by the cold compressed air during the discharging phase. Therefore, in this configuration the use of heat exchangers is avoided.

Fig. 1 and Fig. 2 show the simplified schemes of the two configurations.

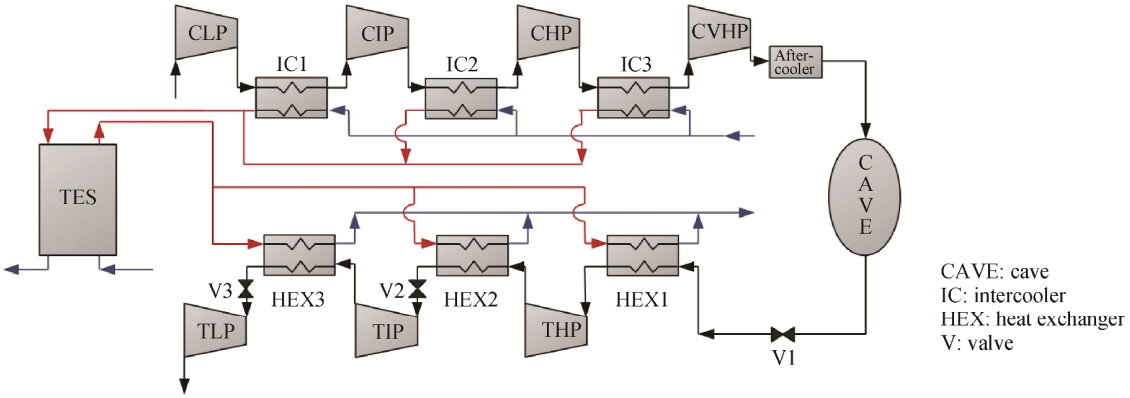


**Fig. 1** Simplified scheme plant of the A-CAES configuration with separated HTF cycle (cases A, B)

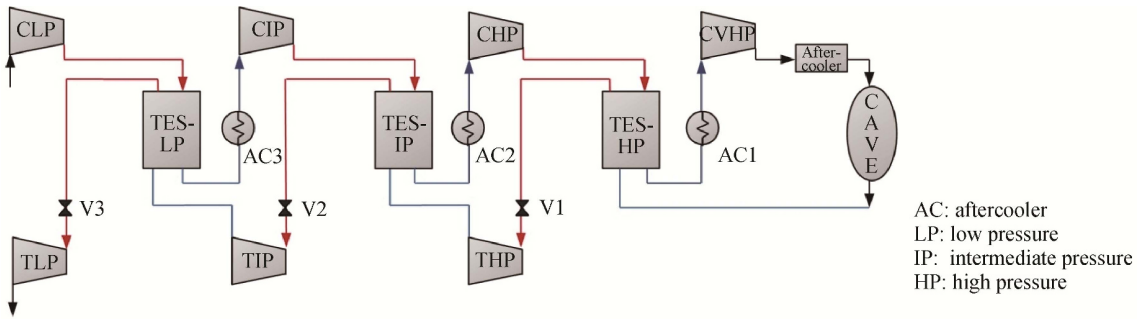


**Fig. 2** Simplified scheme plant of the A-CAES configuration with three TES systems (case C)

### 2.1 Compressors assumptions

The compression train inlet pressure and temperature are set equal to ambient conditions, whereas the air inlet temperature for the subsequent compressors is assumed equal to 35°C. Four centrifugal compressors were considered for both configurations [27]. Table 1 reports the main design parameters of the four compressors.

**Table 1** Main design parameters of the compressors

| | CLP | CIP | CHP | CVHP |
|---|---|---|---|---|
| Inlet pressure/MPa | 0.101 | 0.383 | 1.177 | 3.581 |
| Outlet pressure/MPa | 0.387 | 1.189 | 3.617 | 6.4–10.0 |
| Pressure ratio | 3.8 | 3.1 | 3.1 | 1.8–2.8 |
| Polytropic efficiency | 0.88 | 0.88 | 0.88 | $0.88^*$ |
| Inlet temperature/°C | 15 | 35 | 35 | 35 |
| Outlet temperature/°C | 170 | 170 | 170 | 95–155 |

Note: Subscript * means at nominal conditions.

In all cases, CLP, CIP and CHP work under constant operating conditions and their pressure ratio (3.8, 3.1 and 3.1, respectively) was calculated according to a fixed outlet temperature of 170°C. On the contrary, the CVHP operates as pressure regulator, pressurizing the air inside the CAS from the cave minimum pressure (6.4 MPa) to the maximum one (10.0 MPa), leading to a variable pressure ratio ranging between 1.8 and 2.8. A polytropic efficiency of 0.88 was assumed for the nominal conditions, according to values of commercial turbomachines [21].

In cases A and B, three intercoolers are required to recover the thermal energy at the exit of the first three compressors. Table 2 shows the main design parameters of the intercoolers for cases A and B.

**Table 2** Main design parameters of the intercoolers

| | case A | case B |
|---|---|---|
| HTF | Air | Thermal oil |
| HTF heat capacity*/kJ·kg$^{-1}$·K$^{-1}$ | 1.005 | 1.494 |
| Inlet temperature of the hot fluid/°C | 170 | 170 |
| Minimum temperature difference/°C | 20 | 10 |
| Outlet temperature of the hot fluid/°C | 35 | 35 |

Note: Subscript * means at ambient conditions.

The temperature difference between the operating fluid and the HTF was set according to the fluid: 20°C for air and 10°C for thermal oil. Such temperature difference leads to an outlet temperature of the HTF equal to 150°C and 160°C, respectively. Moreover, an outlet temperature of the hot fluid equal to 35°C was also imposed.

In case C, the heat recovery is directly performed by the operating hot fluid flowing through the TES tanks, allowing the storage of the thermal energy at a higher temperature, equal to the compressor outlet temperature (170°C). However, the outlet temperature of the air exiting the TES system is not constant during the entire charging phase, increasing in the latter part. Therefore, the insertion of an aftercooler downstream of each TES system is required to keep constant the temperature at the inlet of each compressor (35°C) for the entire charging phase, allowing the compressors to operate at design conditions.

### 2.2 Compressed air storage (cave) assumptions

A natural cave was considered as the best option for both configurations. As mentioned, this study doesn't refer to an existing cave and the air pressure variation range inside the cave (6.4–10.0 MPa) was assumed according to typical values of CAES systems. Inside the cave, the air temperature is limited in a range of 15°C–55°C to avoid structural issues.

### 2.3 TES systems assumptions

For both configurations, a sensible heat TES system based on solid storage material (gravel) was considered [28]. The main properties of the storage material are reported in Table 3.

**Table 3** Storage material main properties

| Storage material | Density /kg·m$^{-3}$ | Average particle diameter/m | Specific heat/ kJ·kg$^{-1}$·K$^{-1}$ | Bed void fraction |
|---|---|---|---|---|
| Gravel | 2750 | 0.03 | 0.9 | 0.3 |

The modelling of transient behaviour of the TES systems was performed in the MATLAB-Simulink environment, adapting the two-equation, one-dimensional, transient model developed in Ref. [29], which is based on the model originally developed by Schumann [30]. Starting from the thermo-physical properties of HTF and solid storage material and from tank geometry, the model predicts the time evolution of the spatial distribution of both the HTF and the filling solid material temperature. A more detailed description of the model with the main assumptions can be found in Refs. [16, 31]. A bed void fraction of 0.3 was set, since the gravel was assumed to be composed by particles of different granulometry, some of them even of very small size [32]. The diameter and aspect ratio of each TES system were optimized to reduce the amount of residual thermal energy inside the tank. The design parameters of the TES tanks are reported in Table 4.

Due to the thermocline behaviour, the HTF outlet temperature remains constant for a large part of both charging and discharging phases, increasing (charge) or decreasing (discharge) in the final part. A minimum value

**Table 4** Main parameters of the TES systems

| | case A | case B | case C | | |
|---|---|---|---|---|---|
| | | | TES-LP | TES-IP | TES-HP |
| Operating pressure - charging phase/MPa | 0.101 | 0.101 | 0.39 | 1.19 | 3.68 |
| Operating pressure - discharging phase/MPa | 0.101 | 0.101 | 0.40/0.53 | 1.74/2.24 | 6.40/10.0 |
| Inlet temperature - charging phase/°C | 150 | 160 | 170 | 170 | 170 |
| Outlet temperature - charging phase*/°C | 15 | 15 | 35 | 35 | 35 |
| Inlet temperature - discharging phase/°C | 15 | 15 | 35 | 35 | 35 |
| Outlet temperature - discharging phase*/°C | 150 | 160 | 170 | 170 | 170 |

Note: Subscript * means at nominal conditions.

of the outlet temperature during the discharge equal to 100°C was set for all cases to avoid a large reduction of the turbine performance. No limits were imposed for the outlet temperature during the charging phase.

### 2.4 Turbines assumptions

For both configurations, three radial turbines were selected for the expansion train, as suggested in Ref. [33] for small size plants with a total power output of around 10 MW. The required mass flow of operating fluid was calculated referring to a maximum power output of 10 MW in the most favorable conditions. During the discharging phase, the inlet temperature of each turbine (TIT), ranging between 130°C and 170°C at design conditions, strictly depends on the TES system configuration and behavior. In fact, for a large part of the discharging phase, the TES system allows the turbines to be fed with an air flow rate at constant temperature; conversely, in the final part of the discharging phase the TIT is lower than the nominal one.

In case C, the TIT of each turbine depends only on the outlet temperature of the corresponding TES tank, while in cases A and B the TIT of each turbine depends also on the temperature difference between the operating fluid and the HTF inside the heat exchangers. As previously indicated, this temperature difference was set equal to 20°C in case of air as HTF and to 10°C in the case of thermal oil. Table 5 reports the main parameters of the heat exchangers for case A and case B.

**Table 5** Main design parameters of the heat exchangers

| | case A | case B |
|---|---|---|
| HTF | Air | Oil |
| HTF heat capacity/kJ·kg$^{-1}$·K$^{-1}$ | 1.005 | 1.494 |
| Inlet temperature cold fluid/°C | 15 | 15 |
| Inlet temperature of the hot fluid/°C | 150 | 160 |
| Minimum temperature difference/°C | 20 | 10 |

Table 6 reports the main design parameters of the turbines for the different cases.

**Table 6** Main design parameters of the three turbines

| | case A | case B | case C |
|---|---|---|---|
| Polytropic efficiency | 0.86 | 0.86 | 0.86 |
| On-design inlet temperature/°C | 130 | 150 | 170 |
| Minimum outlet temperature/°C | 15 | 15 | 15 |

The overall pressure ratio of the expansion section is shared out among the three turbines, avoiding an outlet temperature of each turbine lower than 15°C. A valve is placed upstream of each turbine to assure the throttling of the air if this limit cannot be respected.

## 3. Results and Discussion

In this section, the main results of both the charging and the discharging processes are reported.

### 3.1. Compressors operating results

Table 7 reports the power requirements and the global electrical energy consumed during the entire charging process for each compressor. No differences can be noticed among the three studied cases since the compressor train configuration is the same.

The air mass flow rate slightly decreases during the overall compression phase since a small portion of water vapor condensates due to cooling processes. The value of mass flow at the cave inlet was imposed equal to half of the turbine one (24.5 kg/s). Starting from the main parameters of the heat exchangers reported in Table 2, a HTF mass flow rate equal to 38.3 kg/s and 20.1 kg/s was calculated for air (case A) and oil (case B), respectively.

### 3.2 Compressed air storage (cave) operating results

The volume of the cave is the same for all cases and was determined considering the required mass flow of air to achieve the outlet power of 10 MW in the most favorable conditions. Starting from discharge air mass flow (about 24.5 kg/s) and discharge time (3 hours), an overall amount of discharge air equal to 264.6 tons was calculated. With the hypothesis of ideal gas, a cave

volume of 6500 $m^3$ and an air mass at the minimum pressure amounting of about 470 tons were also calculated. Consequently, at the end of the charge the mass of air inside the cavern is equal to about 735 tons.

### 3.3 TES system operating results

In cases A and B, the HTF mass flow entering the TES tanks is the one requested by the heat exchangers to recover the heat from the compressors. Since the discharging phase lasts half the charging phase, the discharging HTF mass flow is doubled. In case C, the TES is directly fed by the operating fluid (about 12.3 kg/s during the charge and 24.5 kg/s during the discharge). An aspect ratio of 2 was set. Table 8 reports the main results of the TES system for the three cases analyzed.

The TES tank was sized starting from the minimum theoretical volume required to store a given amount of energy, without considering the thermocline behavior. Since the hysteresis effects reduce the amount of storable heat, the actual volume is remarkably higher. The volume was calculated by fixing: (a) a complete charging and discharging process (6 and 3 hours, respectively) and (b) a minimum temperature for the outlet air temperature during the discharge equal to 100°C, to avoid an excessive reduction of the turbine power production. No constraints were assumed for the HTF outlet temperature during the charge since each TES system is integrated with an aftercooler to be operated if necessary.

Fig. 3(a)–3(b) show the temperature distribution of the packed bed alongside the tank axis at the end of the charging (red lines) and the discharging phase (blue lines), for both air and thermal oil as HTF, and for a given number of cycles. Fig. 3(c)–3(e) show the same temperature distribution alongside the tank axis for the three TES tanks of case C.

Since the thermocline requires various ($n$) cycles to reach steady-state conditions, the figures report the temperature profile for the first 20 cycles, within which full operational regime is reached in each case. Since the area to the left of a charging curve represents an index of the storable energy, while the area to the left of a discharging one represents an index of the residual energy, globally, for each cycle, the area between these curves represents an index of the useful thermal energy released by the storage system. Conventionally, in Fig. 3(a)–3(e), the zero value of the tank height corresponds to the upper section, where the hottest HTF enters during the charging phase and exits during the discharging phase.

Fig. 3(a)–3(e) show that the number of cycles required by the TES system to converge to stable conditions depends on both the chosen HTF and the configuration. As shown in Fig. 3(a)–3(b), in the first configuration, the use of air as HTF leads to a faster convergence than oil, due to the lower storage capacity and thus air allows to achieve quickly stable conditions after a plant shutdown. Furthermore, for all the cases, only the first charging cycle shows a remarkable difference of the temperature profile since it starts with a fully empty tank. Figures show that, as for the charge, during the discharge, the HTF outlet temperature increases with the cycle number, leading to a higher TIT and, consequently, to a greater energy production by the turbines. In particular, the HTF outlet temperature at the end of discharge is equal to 100°C (initial set value) in the first cycle, but it swiftly increases with the number of cycles. During the charging phase, a higher temperature allows the charge level of the TES system to be increased, even if a greater amount of

**Table 7** Power and energy requirements during the charging phase

| | CLP | CIP | CHP | CVHP | Overall |
|---|---|---|---|---|---|
| Air mass flow/kg·s$^{-1}$ | 12.35 | 12.35 | 12.31 | 12.28 | – |
| Power requirements/MW | 1.98 | 1.73 | 1.72 | 0.79–1.55 | 6.22–6.98 |
| Electrical energy/MWh | 11.90 | 10.38 | 10.31 | 7.16 | 39.76 |

**Table 8** Main results of the TES system

| | case A | case B | case C | | |
|---|---|---|---|---|---|
| | | | TES-LP | TES-IP | TES-HP |
| Tank diameter/m | 7.5 | 7 | 5.2 | 5.2 | 5.2 |
| Aspect ratio | 2 | 2 | 2 | 2 | 2 |
| Volume/$m^3$ | 663 | 539 | 220.8 | 220.8 | 220.8 |
| Charging phase mass flow/kg·s$^{-1}$ | 38.3 | 20.1 | 12.3 | 12.3 | 12.3 |
| Discharging phase mass flow/kg·s$^{-1}$ | 76.6 | 40.2 | 24.5 | 24.5 | 24.5 |
| Inlet temperature charging phase/°C | 150 | 160 | 170 | 170 | 170 |
| Inlet temperature discharging phase/°C | 15 | 15 | 35 | 35 | 35 |
| Stored energy/MWh | 29.93 | 29.98 | 9.60 | 9.54 | 9.54 |

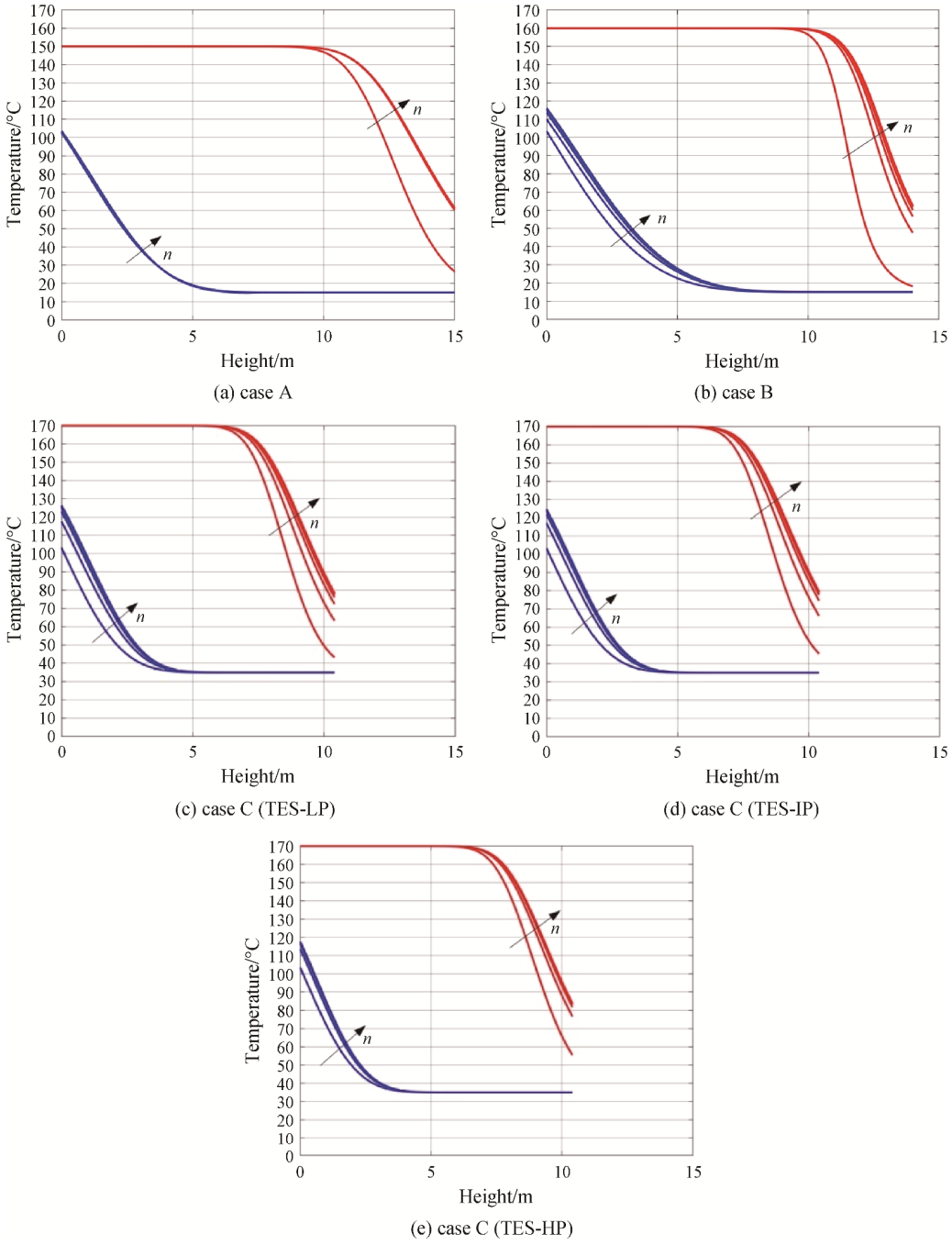


**Fig. 3** Temperature profile inside the TES tank

thermal energy must be dissipated if a HTF low temperature is required, as in case C, where the HTF directly feeds the subsequent compressor.

Fig. 4(a) and 4(b) show the air temperature at the outlet of the TES tanks as a function of time for the charging and discharging phases, respectively.

As shown in Fig. 4(a) and 4(b), the HTF temperature at the outlet of the TES tanks remains constant at the nominal value for about two thirds of the duration of both charging and discharging phases. In the latter part, the temperature starts to increase (charging phase) or decrease (discharging phase) affecting the operation of the turbomachines. In the first configuration (cases A and B), the TES behaviour affects only the operation of turbines, while in the second one (case C) it also influences the operation of compressors, being the TES directly connected to both compressors and turbines. Hence, case C requires to insert an aftercooler before each compressor to keep the value of the air temperature constant at the compressor inlet.

### 3.4 Turbines operating results

The turbines behaviour is directly influenced by the TES system operation. In the first two hours of the discharging phase the air inlet temperature is almost constant; on the contrary, in the last one the air temperature becomes lower than the on-design one, affecting the turbines operation.

Fig. 5(a)–5(d) report for each turbine of case A: (a) the inlet and outlet temperature, (b) the inlet and outlet pressure, (c) the corresponding pressure ratio $\beta$, and (d) the power output.

As shown in Fig. 5(a), the turbine inlet temperature (TIT) of each turbine is equal to 130°C for more than half of the duration of the discharge, while later it is reduced to a minimum value slightly higher than 80°C. Such a low TIT requires a throttling process to respect the minimum value of 15°C of the high-pressure turbine outlet temperature (TOT). As shown in Fig. 5(b), right from the beginning of the discharge, the valve reduces the inlet pressure of the THP down to about 6.5 MPa, and a further reduction is required when the TIT starts to decrease. Since the water vapor content is almost negligible, the air shows a behavior very similar to that of the ideal gas and its temperature reduction is limited to a few tenths of Celsius degrees. Moreover, the reduction of the air temperature takes place at the inlet of the heat

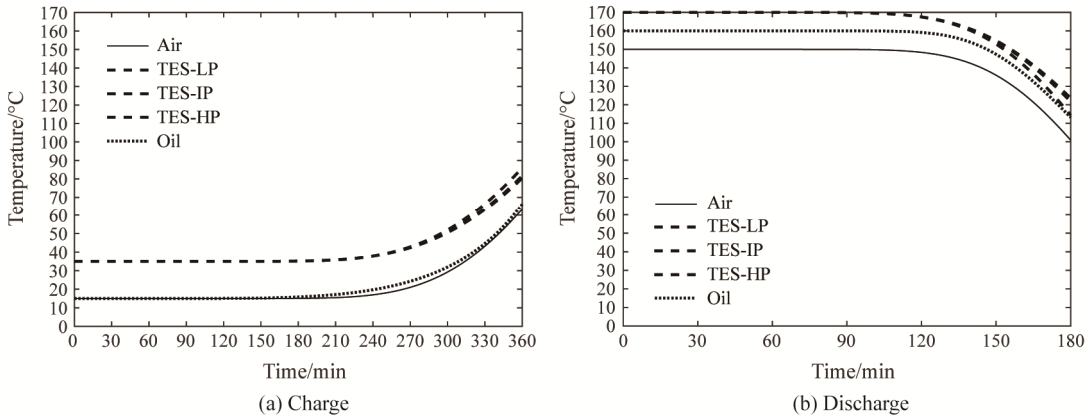


**Fig. 4** Outlet temperature of air from the TES system

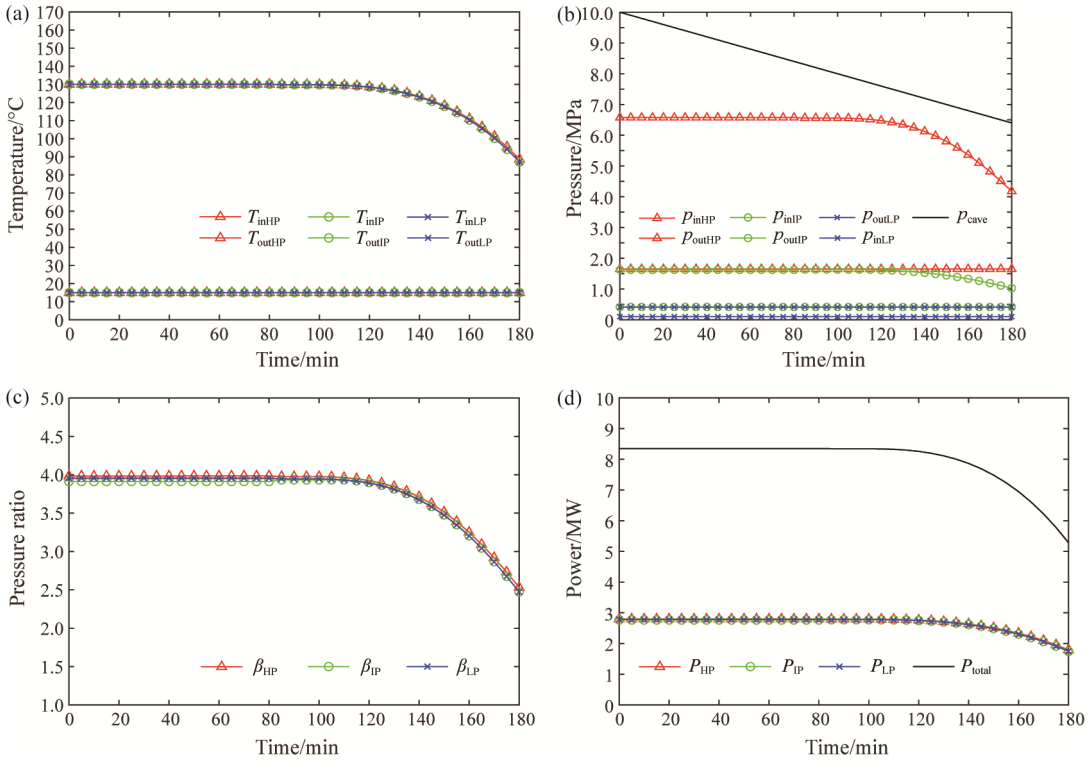


**Fig. 5** Main performance of the turbines for case A

exchanger and, consequently, a constant air outlet temperature of 130°C was assumed to be reached at the THP inlet. At the same time, the TIT reduction also requires a throttling upstream of both TIP and TLP, reducing the pressure ratios from a nominal value of about 4 to a minimum value of about 2.5 at the end of the discharge, as shown by Fig. 5(c). As expected, the reduction of pressure ratio $\beta$ leads to a performance penalization for the turbines. Fig. 5(d) shows that the power production of each turbine is reduced from a maximum value slightly lower than 3 MW to a minimum value of about 1.75 MW. Globally, for case A, the overall power production reaches a maximum value of around 8.3 MW and it is reduced to about 5.3 MW at the end of the discharge.

Fig. 6(a)–6(d) report for each turbine of case B: (a) the inlet and outlet temperature, (b) the inlet and outlet pressure, (c) the corresponding pressure ratio $\beta$, and (d) the power output.

Differently from case A, thanks to the higher TES systems temperature, case B allows to fully exploit the overall pressure ratio between cave and ambient without operating the throttling valves until the last half an hour of the discharging phase. During the first part of the discharging phase, when the TES system operates at nominal conditions assuring a TIT of 150°C, the TOT of both THP and TIP is kept constant to the minimum value of 15°C with a constant pressure ratio of both high- and intermediate-pressure turbines, namely $\beta_{HP}$ and $\beta_{IP}$. Therefore, the reduction of the cave pressure leads to a lower pressure ratio $\beta_{LP}$ of the TLP and consequently to a higher TOT of the TLP as shown in Fig. 6(a). As soon as TIT starts to decrease, both $\beta_{HP}$ and $\beta_{IP}$ decrease, and consequently $\beta_{LP}$ increases, leading to a lower TOT of the TLP. In the last half an hour, the TOT of the TLP would decrease down to 15°C, requiring the throttling valve to be operated and, consequently, $\beta_{LP}$ exhibits the same behavior as $\beta_{HP}$ and $\beta_{IP}$, as shown by Fig. 6(c). Fig. 6(d) shows that the power production of both THP and TIP is higher than 3 MW for a large part of the discharging phase, while the power production of the TLP is lower than 3 MW. During the last half an hour, all three power outputs decrease to a minimum of about 2 MW. Globally, for case B, the overall power output shows an initial value of 9.5 MW and gradually decreases by about 6 kW/min. However, during the last twenty minutes, the power output sharply decreases to about 6.3 MW.

Finally, Fig. 7(a)–7(d) report for each turbine of case C: (a) the inlet and outlet temperature, (b) the inlet and outlet pressure, (c) the corresponding pressure ratio $\beta$, and (d) the power output.

Fig. 7(a) shows that, thanks to a higher TIT (170°C at TES nominal conditions), in case C a constant outlet temperature of 35°C for both THP and TIP can be achieved for almost all the duration of the discharge, without any effect on the operation of TES-IP and TES-LP. As in case B, the overall pressure ratio between cave and ambient can be fully exploited without

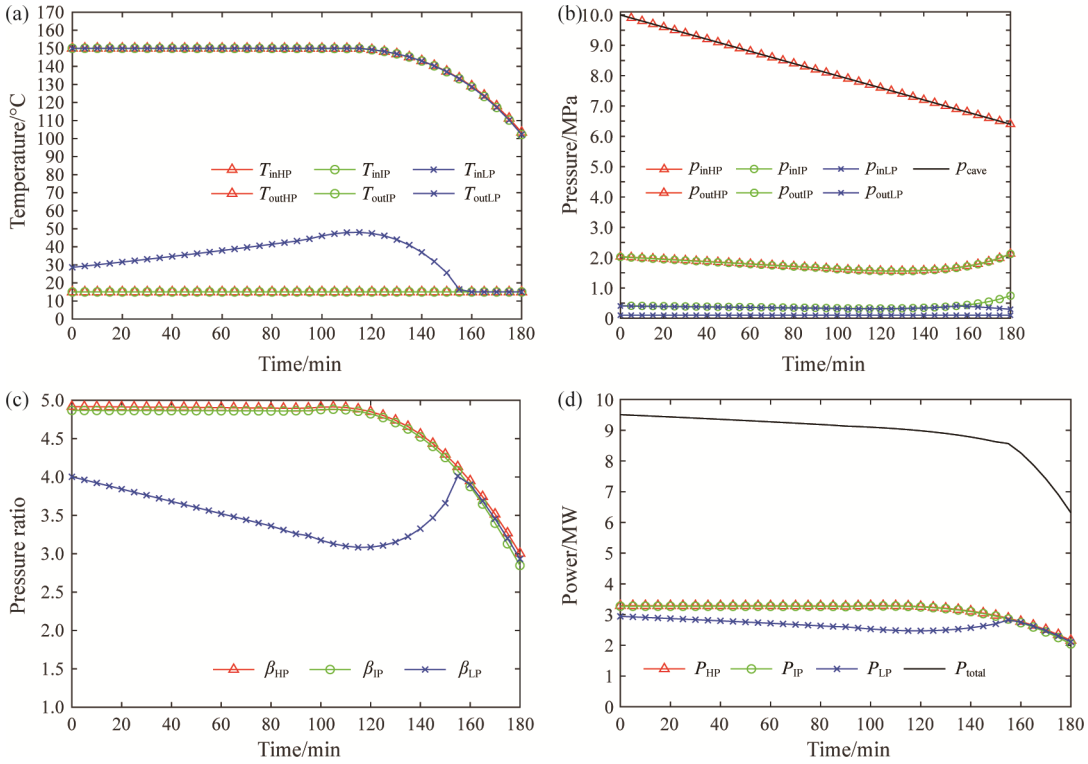


**Fig. 6** Main performance of the turbines for case B

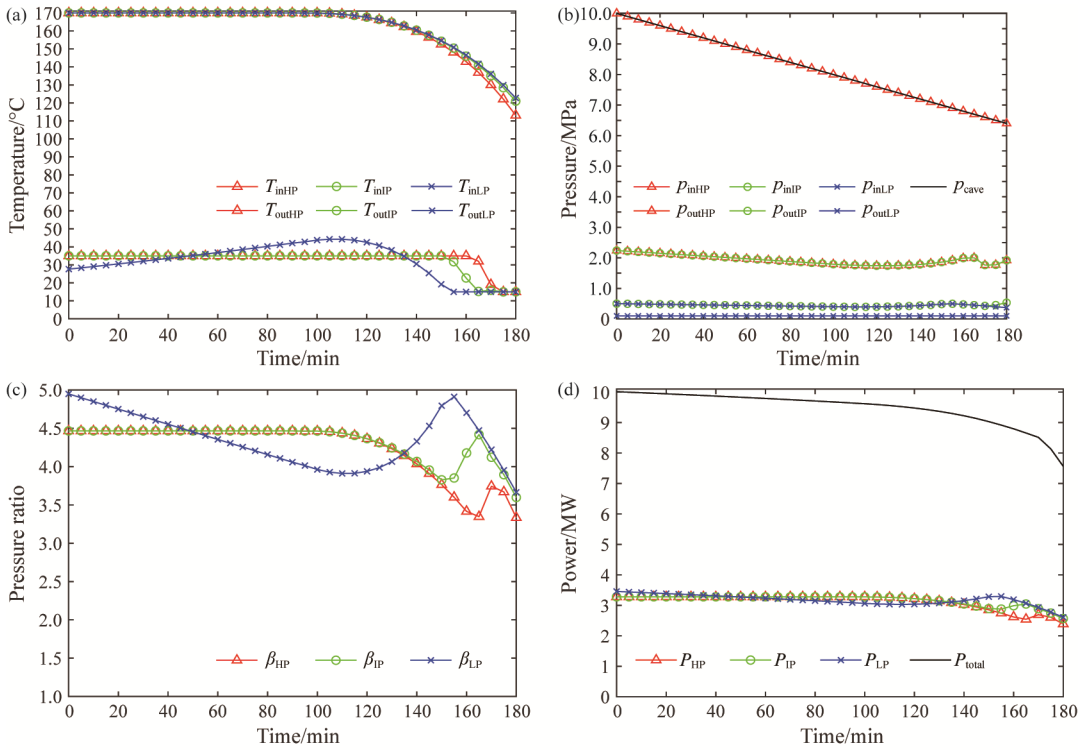


**Fig. 7** Main performance of the turbines for case C

operating the throttling valves for the largest part of the discharging process, except for the low-pressure turbine during the last 5 minutes, as shown in Fig. 7(b). In fact, the reduction of the cave pressure leads to a lower $\beta_{LP}$ (Fig. 7(c)) and consequently to a higher TOT of the TLP (Fig. 7(a)). When the TIT begins to decrease, both $\beta_{HP}$ and $\beta_{IP}$ start to decrease too, leading to a $\beta_{LP}$ increase and a consequent TOT decrease. In the last half an hour, the TOT of the TLP reaches 15°C, resulting in a TOT reduction also for both THP and TIP. Just in the final 5 minutes, when the outlet temperature of the three turbines reaches the minimum of 15°C, a throttling occurs in the low-pressure valve. Fig. 7(d) shows that the power production is higher than 3 MW for all the turbines during a large part of the discharge. Globally, for case C, the overall power shows an initial value of 10 MW and gradually decreases to about 7.6 MW.

Table 9 summarizes for the three cases the power production of each turbine and the overall energy production during the full discharging process.

As shown in Table 9, due to the lower TIT, case A and case B lead to a lower power production (8.3 and 9.5 MW as maximum value, respectively) than the reference value of 10 MW, set for case C. In particular, in case A the throttling valve upstream of the high-pressure turbine starts to operate at the beginning of the discharging phase, sensibly affecting the power production, while in case B the difference is less significant, except for the low-pressure turbine and the last part of the discharging process. Globally, for the three hours of discharge, a minimum value of the overall energy production equal to 23.9 MWh can be noticed for case A, whereas case C allows an overall energy production of 28.5 MWh.

**Table 9** Power and energy production

| | THP | TIP | TLP | Overall |
|---|---|---|---|---|
| | Power production/MW | | | |
| case A | 2.8–1.8 | 2.8–1.7 | 2.8–1.7 | 8.3–5.3 |
| case B | 3.3–2.2 | 3.3–2.1 | 2.9–2.1 | 9.5–6.3 |
| case C | 3.3–2.4 | 3.3–2.6 | 3.4–2.6 | 10.0–7.6 |
| | Energy production/MWh | | | |
| case A | 8.02 | 7.94 | 7.96 | 23.92 |
| case B | 9.46 | 9.38 | 7.97 | 26.82 |
| case C | 9.41 | 9.53 | 9.54 | 28.48 |

## 4. Performance Comparison of the Different Solutions

In order to compare the performance of the different LT-ACAES solutions, a round-trip efficiency was introduced. The round-trip efficiency is defined as the ratio between the electrical energy generated by the turbines and the one required by the compressor train. A motor/generator efficiency equal to 0.97 was set to convert the mechanical energy of both compressors and turbines into electrical energy. Table 10 summarizes the main overall results for the three cases.

**Table 10** Main overall results of each configuration

| | case A | case B | case C |
|---|---|---|---|
| Air mass flow - charging phase*/kg·s$^{-1}$ | 12.35 | 12.35 | 12.35 |
| Air mass flow - discharging phase/kg·s$^{-1}$ | 24.50 | 24.50 | 24.50 |
| HTF mass flow - charging phase/kg·s$^{-1}$ | 38.3 | 20.1 | 12.25 |
| Overall tanks volume/m$^3$ | 663.0 | 539.0 | 662.4 |
| TES tank operating temperature/°C | 150 | 160 | 170 |
| Compressor overall power/MW | 6.2–6.9 | 6.2–6.9 | 6.2–6.9 |
| Maximum turbines overall power/MW | 8.3 | 9.5 | 10.0 |
| Compressors energy requirement/MWh | 39.8 | 39.8 | 39.8 |
| Turbines energy production/MWh | 23.9 | 26.8 | 28.5 |
| Round-trip efficiency | 0.566 | 0.635 | 0.674 |

Note: Subscript * means at low-pressure compressor inlet.

To reach a power production of 10 MW with the most favorable configuration, an air mass flow rate equal to 24.5 kg/s is required in the expansion train. Such mass flow rate leads to a mass flow in the compression train about half of the expansion train one, due to the charge-to-discharge duration ratio.

In the first configuration (cases A and B), the use of air as HTF leads to a larger volume of the TES tank (663 m$^3$) compared to the one required by thermal oil (539 m$^3$), thanks to the contribution of oil to thermal storage. The lower volumetric heat capacity of the air as HTF also leads to a greater mass flow rate. The overall volume of the three TES tanks of case C (662.4 m$^3$) is about the same as the tank volume of the case A.

Since the system was designed with the same size for the compression and air storage sections independently from the configuration, the power and energy requirements for the compressors during the charging phase result the same for all the cases studied. Consequently, the round-trip efficiency only depends on the energy production of the turbines during the discharging phase. As shown in Table 10, the round-trip efficiency of the LT-ACAES configurations studied ranges between 0.566 (case A) to 0.674 (case C).

## 5. Conclusions

Energy storage systems can play an important role in the context of energy production and distribution, especially with the widespread diffusion of renewable energy sources. In this framework, low-temperature A-CAES plants appear to be an effective solution to store electrical energy for small and medium scale applications.

In this paper, two LT-ACAES configurations with different heat recovery solutions were studied, the main difference being the system used to recover, store, and utilize the thermal energy during the charging and discharging phases. For both configurations, a sensible TES system with solid storage material was considered to store the thermal energy. In the first configuration, a heat transfer fluid recovers thermal energy from the compressor intercooling and it is then used to heat the air at the turbine inlet requiring the introduction of several heat exchangers. Two different HTFs were considered: air (case A) and thermal oil (case B). On the other hand, in the second configuration the TES system (based on three tanks operating at different pressure) is directly connected to the turbomachinery, so the use of heat exchangers is avoided.

In the first configuration, the presence of the heat exchangers leads to a greater complexity of the plant design and higher costs. However, in the second one, the three TES tanks operate at increasing pressure with consequent structural issues, so the design and the maintenance of the tanks require a particular attention. Besides, the first configuration allows separating the operating fluid and the HTF cycles, with the possibility to use HTF different from air for the TES. The use of thermal oil leads to a smaller tank volume (lower than 540 m$^3$ in comparison to a volume higher than 660 m$^3$ in the case of air as HTF) and better plant performance (a round-trip efficiency of 0.635 was calculated, 7 percentage points higher than that of case A), due to its lower temperature difference inside the heat exchangers, however it also requires a closed cycle with the insertion of an additional tank to store the cold oil. On the contrary, one of the main advantages of using air as HTF is the possibility to realize an open cycle for the HTF with only one TES tank, making air as HTF a more sustainable choice.

The second configuration with three TES systems appears to be the most promising in terms of round-trip efficiency since the energy produced during the discharging phase is greater, due to the higher temperature inside the TES. The round-trip efficiency of the case C is slightly lower than 0.65.

To conclude, this study is a preliminary analysis of the performance of different LT-ACAES configurations and it is expected to be integrated with a technical-economic analysis that takes into account all the aspects of the LT-ACAES design. Moreover, although the second configuration leads to unquestionable better performance, the effect of operating at very high pressures inside the tanks should be carefully analysed in relation to the overall cost of the system.

## Acknowledgments

This work was carried out in the framework of the Research Projects: (a) RASSR07979 “Development of a hybrid energy storage system for ancillary services devoted in power systems”, funded by the Sardinia Region and (b) “Advanced Energy Storage Systems for Sustainable Communities” supported by “Fondazione di Sardegna”.

## References

[1] https://www.iea.org/reports/renewable-power 2021. https://www.iea.org/reports/renewable-power (accessed October 29, 2021).

[2] Hu S., Liu C., Ding J., Xu Y., Chen H., Zhou X., Thermo-economic modeling and evaluation of physical energy storage in power system. Journal of Thermal Science, 2021, 30: 1–14.
DOI: 10.1007/s11630-021-1417-4.

[3] Ould Amrouche S., Rekioua D., Rekioua T., Bacha S., Overview of energy storage in renewable energy systems. International Journal of Hydrogen Energy, 2016, 41: 20914–20927.
DOI: 10.1016/j.ijhydene.2016.06.243.

[4] Koohi-Fayegh S., Rosen M.A., A review of energy storage types, applications and recent developments. Journal of Energy Storage, 2020, 27: 101047.
DOI: 10.1016/j.est.2019.101047.

[5] IEA Report. Technology roadmap: Energy storage. 2014.

[6] Budt M., Wolf D., Span R., Yan J., A review on compressed air energy storage: Basic principles, past milestones and recent developments. Applied Energy, 2016, 170: 250–268.
DOI: 10.1016/j.apenergy.2016.02.108.

[7] Das C.K., Bass O., Kothapalli G., Mahmoud T.S., Habibi D., Overview of energy storage systems in distribution networks: Placement, sizing, operation, and power quality. Renewable Sustainable Energy Review, 2018, 91: 1205–1230.
DOI: 10.1016/j.rser.2018.03.068.

[8] Crotogino F., Mohmeyer K.U., Scharf R., Huntorf CAES: More than 20 years of successful operation. Solution Mining Research Institute Spring Meeting, Orlando, 23–25 April, 2001, pp. 351–357.

[9] De Biasi V., 110 MW McIntosh CAES plant over 90% availability and 95% reliability. Gas Turbine World, 1998, 28: 26–28.

[10] Song J., Peng X., Fang X., Han Y., Deng Z., Xu G., et al., Thermodynamic analysis and algorithm optimisation of a multi-stage compression adiabatic compressed air energy storage system. Thermal Science and Engeneering Progess, 2020, 19: 100598.
DOI: 10.1016/j.tsep.2020.100598.

[11] Li Y., Miao S., Zhang S., Yin B., Luo X., Dooner M., et al., A reserve capacity model of AA-CAES for power system optimal joint energy and reserve scheduling. International Journal of Electrical Power & Energy Systems, 2019, 104: 279–290.
DOI: 10.1016/j.ijepes.2018.07.012.

[12] Tong S., Cheng Z., Cong F., Tong Z., Zhang Y., Developing a grid-connected power optimization strategy for the integration of wind power with low-temperature adiabatic compressed air energy storage. Renewable Energy, 2018, 125: 73–86.
DOI: 10.1016/j.renene.2018.02.067.

[13] Hartmann N., Vöhringer O., Kruck C., Eltrop L., Simulation and analysis of different adiabatic Compressed Air Energy Storage plant configurations. Appied Energy, 2012, 93: 541–548.
DOI: 10.1016/j.apenergy.2011.12.007.

[14] Wang S., Zhang X., Yang L., Zhou Y., Wang J., Experimental study of compressed air energy storage system with thermal energy storage. Energy, 2016, 103: 182–191. DOI: 10.1016/j.energy.2016.02.125.

[15] Liu J., Zhang X., Xu Y., Chen Z., Chen H., Tan C., Economic analysis of using above ground gas storage devices for compressed air energy storage system. Journal of Thermal Science, 2014, 23: 535–543.
DOI: 10.1007/s11630-014-0738-y.

[16] Tola V., Meloni V., Spadaccini F., Cau G., Performance assessment of Adiabatic Compressed Air Energy Storage (A-CAES) power plants integrated with packed-bed thermocline storage systems. Energy Conversion and Management, 2017, 151: 343–356.
DOI: 10.1016/j.enconman.2017.08.051.

[17] Raju M., Kumar Khaitan S., Modeling and simulation of compressed air storage in caverns: A case study of the Huntorf plant. Applied Energy, 2012, 89: 474–481.
DOI: 10.1016/j.apenergy.2011.08.019.

[18] Zhou Q., Du D., Lu C., He Q., Liu W., A review of thermal energy storage in compressed air energy storage system. Energy, 2019, 188: 115993.
DOI: 10.1016/j.energy.2019.115993.

[19] Zhao P., Dai Y., Wang J., Design and thermodynamic

analysis of a hybrid energy storage system based on A-CAES (adiabatic compressed air energy storage) and FESS (flywheel energy storage system) for wind power application. Energy, 2014, 70: 674–684.
DOI: 10.1016/j.energy.2014.04.055.

[20] Castellani B., Presciutti A., Filipponi M., Nicolini A., Rossi F., Experimental investigation on the effect of phase change materials on compressed air expansion in CAES plants. Sustainability, 2015, 7: 9773–9786.
DOI: 10.3390/su7089773.

[21] Barbour E., Mignard D., Ding Y., Li Y., Adiabatic Compressed Air Energy Storage with packed bed thermal energy storage. Applied Energy, 2015, 155: 804–815.
DOI: 10.1016/j.apenergy.2015.06.019.

[22] Alva G., Lin Y., Fang G., An overview of thermal energy storage systems. Energy, 2018, 144: 341–378.
DOI: 10.1016/j.energy.2017.12.037.

[23] Wolf D., Budt M., LTA-CAES - A low-temperature approach to adiabatic compressed air energy storage. Applied Energy, 2014, 125: 158–164.
DOI: 10.1016/j.apenergy.2014.03.013.

[24] Luo X., Wang J., Krupke C., Wang Y., Sheng Y., Li J., et al., Modelling study, efficiency analysis and optimisation of large-scale Adiabatic Compressed Air Energy Storage systems with low-temperature thermal storage. Applied Energy, 2016, 162: 589–600.
DOI: 10.1016/j.apenergy.2015.10.091.

[25] Guo C., Xu Y., Guo H., Zhang X., Lin X., Wang L., et al., Comprehensive exergy analysis of the dynamic process of compressed air energy storage system with low-temperature thermal energy storage. Applied Thermal Engineering, 2019, 147: 684–693.
DOI: 10.1016/j.applthermaleng.2018.10.115.

[26] Guo H., Xu Y., Guo C., Zhang Y., Hou H., Chen H., Off-design performance of CAES systems with low-temperature thermal storage under optimized operation strategy. Journal of Energy Storage, 2019, 24: 100787.
DOI: 10.1016/j.est.2019.100787.

[27] Brown R.N., Compressors: Selection and Sizing. 3rd Edition, January 2005. Elsevier Science & Technology, Ansterdam.

[28] Guo H., Xu Y., Guo C., Chen H., Wang Y., Yang Z., et al., Thermodynamic analysis of packed bed thermal energy storage system. Journal of Thermal Science, 2020, 29: 445–456. DOI: 10.1007/s11630-019-1115-7.

[29] Cascetta M., Cau G., Puddu P., Serra F., Numerical investigation of a packed bed thermal energy storage system with different heat transfer fluids. Energy Procedia, 2014, 45: 598–607.
DOI: 10.1016/j.egypro.2014.01.064.

[30] Schumann T.E.W., Heat transfer: a liquid flowing porous prism. Journal of Franklin Institute, 1929, 208: 405–416.

[31] Cascetta M., Serra F., Cau G., Puddu P., Comparison between experimental and numerical results of a packed-bed thermal energy storage system in continuous operation. Energy Procedia, 2018, 148: 234–241.

[32] Bruch A., Molina S., Esence T., Fourmigué J.F., Couturier R., Experimental investigation of cycling behaviour of pilot-scale thermal oil packed-bed thermal storage system. Renewable Energy, 2017, 103: 277–285.
DOI: 10.1016/j.renene.2016.11.029.

[33] He W., Wang J., Optimal selection of air expansion machine in Compressed Air Energy Storage: A review. Renewable Sustainable Energy Review, 2018, 87: 77–95.
DOI: 10.1016/j.rser.2018.01.013.